The Endocytosis of Cellulose Synthase in Arabidopsis Is Dependent on μ2, a Clathrin-Mediated Endocytosis Adaptin[1][W][OPEN]

Logan Bashline, Shundai Li, Charles T. Anderson, Lei Lei, and Ying Gu*

Center for Lignocellulose Structure and Formation (L.B., S.L., C.T.A., L.L., Y.G.), Department of Biochemistry and Molecular Biology (L.B., S.L., L.L., Y.G.), and Department of Biology (C.T.A.), Pennsylvania State University, University Park, Pennsylvania 16802

Clathrin-mediated endocytosis (CME) is the best-characterized type of endocytosis in eukaryotic cells. Plants appear to possess all of the molecular components necessary to carry out CME; however, functional characterization of the components is still in its infancy. A yeast two-hybrid screen identified μ2 as a putative interaction partner of CELLULOSE SYNTHASE6 (CESA6). Arabidopsis (*Arabidopsis thaliana*) μ2 is homologous to the medium subunit 2 of the mammalian ADAPTOR PROTEIN COMPLEX2 (AP2). In mammals, the AP2 complex acts as the central hub of CME by docking to the plasma membrane while concomitantly recruiting cargo proteins, clathrin triskelia, and accessory proteins to the sites of endocytosis. We confirmed that μ2 interacts with multiple CESA proteins through the μ-homology domain of μ2, which is involved in specific interactions with endocytic cargo proteins in mammals. Consistent with its role in mediating the endocytosis of cargos at the plasma membrane, μ2-YELLOW FLUORESCENT PROTEIN localized to transient foci at the plasma membrane, and loss of μ2 resulted in defects in bulk endocytosis. Furthermore, loss of μ2 led to increased accumulation of YELLOW FLUORESCENT PROTEIN-CESA6 particles at the plasma membrane. Our results suggest that CESA represents a new class of CME cargo proteins and that plant cells might regulate cellulose synthesis by controlling the abundance of active CESA complexes at the plasma membrane through CME.

Cellulose microfibrils, as the major load-bearing polymers in plant cell walls, are the predominant component that enforces asymmetric cell expansion (Green, 1962). In higher plants, cellulose is synthesized by multimeric rosettes, which are also referred to as cellulose synthase complexes (CSCs; Kimura et al., 1999). Genetic and coimmunoprecipitation studies have indicated that CELLULOSE SYNTHASE1 (CESA1), CESA3, and CESA6-like (CESA6, CESA2, CESA5, and CESA9) isoforms are constituents of CSCs during primary cell wall synthesis (Persson et al., 2005; Desprez et al., 2007; Persson et al., 2007; Wang et al., 2008), whereas CESA4, CESA7, and CESA8 are implicated in the cellulose synthesis of secondary cell walls (Taylor et al., 1999, 2003; Brown et al., 2005). Knowledge about cellulose synthesis has recently been enhanced by the development of a system whereby the dynamics of CESA can be imaged in living cells (Paredez et al., 2006; Desprez et al., 2007). In agreement with earlier transmission electron microscopy studies in which rosettes were visualized in Golgi cisternae, vesicles, and at the plasma membrane (Haigler and Brown, 1986), fluorescent protein tagging of CESA has identified CESA localization at the plasma membrane, in Golgi bodies, and in small intracellular compartments (Paredez et al., 2006; Desprez et al., 2007; Crowell et al., 2009; Gutierrez et al., 2009; Gu et al., 2010; Lei et al., 2012; Li et al., 2012b).

Assuming that cellulose synthesis occurs solely at the plasma membrane, the trafficking of CSCs to and from the plasma membrane may act as a significant regulatory mechanism. Although the mechanistic details of CESA trafficking are lacking, live cell imaging has shown that CESA localizes to various subcellular compartments. A subset of CESAs colocalize with markers of the trans-Golgi network (TGN)/early endosome (EE), an organelle that is part of both the secretory and endocytic pathways in Arabidopsis (*Arabidopsis thaliana*; Dettmer et al., 2006; Lam et al., 2007; Crowell et al., 2009, 2010; Viotti et al., 2010). CESAs also localize to microtubule-associated cellulose synthase compartments (MASCs) and small CESA-containing compartments (SmaCCs). The exact function of SmaCCs/MASCs is unknown, but it has been proposed that SmaCCs/MASCs might result from the internalization of CSCs or might act in the delivery of CSCs to the plasma membrane (Crowell et al., 2009, 2010; Gutierrez et al., 2009).

Clathrin-mediated endocytosis (CME) has been shown to be a major endocytic pathway in Arabidopsis (Holstein, 2002; Samaj et al., 2005; Dhonukshe et al.,

[1] This work was supported by the Center for LignoCellulose Structure and Formation, an Energy Frontier Research Center funded by the U.S. Department of Energy, Office of Science, Office of Basic Sciences (grant no. DE–SC0001090).

* Address correspondence to yug13@psu.edu.

The author responsible for distribution of materials integral to the findings presented in this article in accordance with the policy described in the Instructions for Authors (www.plantphysiol.org) is: Ying Gu (yug13@psu.edu).

[W] The online version of this article contains Web-only data.

[OPEN] Articles can be viewed online without a subscription.

www.plantphysiol.org/cgi/doi/10.1104/pp.113.221234

2007; Kleine-Vehn and Friml, 2008; Chen et al., 2011; Beck et al., 2012; Wang et al., 2013), although there is also evidence of clathrin-independent endocytosis mechanisms (Bandmann and Homann, 2012). The function of many CME proteins has been extensively characterized in mammals (McMahon and Boucrot, 2011), and homologs of many CME components are encoded by the Arabidopsis genome, including multiple copies of clathrin H chain and clathrin light chain (CLC), all four subunits of the heterotetrameric ADAPTOR PROTEIN COMPLEX2 (AP2) complex, dynamin-related proteins, and accessory proteins such as AP180 (Holstein, 2002; Chen et al., 2011); however, many CME components have yet to be characterized in plants.

It has been suggested that CME might also function in controlling cell wall metabolism. For example, dividing and growing cells internalize cross-linked cell wall pectins, which might allow for cell wall remodeling (Baluska et al., 2002, 2005; Samaj et al., 2004). Moreover, the importance of endocytosis for cell wall morphogenesis is apparent from the functional characterization of proteins involved in CME. A dynamin-related protein, DRP1A, plays a significant role in endocytosis and colocalizes with CLC (Collings et al., 2008; Konopka and Bednarek, 2008). Defective endocytosis in *RADIAL SWELLING9* (*rsw9*) plants, which contain a mutation in *DRP1A*, results in cellulose deficiency and defects in cell elongation (Collings et al., 2008). A mutation in rice, *brittle culm3* (*bc3*), was mapped to the dynamin-related gene *OsDRP2A*, which has been proposed to function in CME. The brittle-culm phenotype in this mutant was attributed to cellulose deficiency (Xiong et al., 2010). Although the abundance of OsCESA4 was also altered in *bc3*, it remains unclear whether the cellulose deficiency of either *bc3* or *rsw9* results directly from perturbations in CESA trafficking.

To identify proteins involved in the regulation of cellulose biosynthesis, a yeast two-hybrid (Y2H) screen was performed in which the central domain of CESA6 (CESA6CD) was used as bait to screen an Arabidopsis complementary DNA library for potential interaction partners of CESA6 (Gu et al., 2010; Gu and Somerville, 2010). The Y2H screen identified μ2 as a putative interaction partner of CESA6CD. The mammalian homolog of μ2 is the medium subunit of the tetrameric AP2, which acts as the core of the CME machinery by docking to the plasma membrane while concomitantly recruiting cargo proteins, clathrin triskelia, and accessory proteins to the sites of endocytosis (Jackson et al., 2010; McMahon and Boucrot, 2011; Cocucci et al., 2012). In this study, we provide evidence that μ2 plays a role in CME in Arabidopsis, that CESAs are a new set of CME cargo proteins, and that plant cells might regulate cellulose synthesis by controlling the abundance of CSCs at the plasma membrane through CME. To our knowledge, this study is the first to show the affect of an AP2 complex component on endocytosis in plants and the first to visualize an AP2 complex component in living plant cells. Furthermore, our data suggest that the role of AP2 in plants may differ from what has been shown in animals.

RESULTS

μ2 Directly Interacts with CESA Proteins

μ2 was identified as a putative interaction partner of the central domain of CESA6 in a conventional Y2H screen (Supplemental Fig. S1). In mammals, the N-terminal domain of μ2 mediates its association with the AP2 complex, whereas the C-terminal μ-homology domain of μ2 (μ2MHD) is involved in specific interactions with endocytic cargo proteins (Supplemental Fig. S2A; Jackson et al., 2010). To investigate the cargo-binding role of μ2, both full-length μ2 and μ2MHD were tested for direct interaction with full-length CESA3 and CESA6 using the split-ubiquitin (SU)-Y2H assay, which can analyze protein-protein interactions of integral membrane proteins (Obrdlik et al., 2004). In the SU-Y2H screen, reconstitution of a functional ubiquitin from its N-terminal (Nub) and C-terminal (Cub) halves is recognized by ubiquitin-specific proteases, which cleave a fused transcription factor module (PLV) from the Cub to activate the expression of LexA-driven reporter genes, HIS3 and LacZ, in the nucleus. Wild-type Nub (NubWT) readily binds to the Cub of the CESA3-Cub-PLV and CESA6-Cub-PLV bait constructs and was used as a positive control (Fig. 1A, columns 1 and 3). A mutated form of Nub (NubG) has a reduced affinity for binding to Cub and was used as a negative control with the bait constructs (Fig. 1A, columns 2 and 4). When either μ2 or μ2MHD was fused to NubG and cotransformed into yeast (*Saccharomyces cerevisiae* strain THY.AP4) with CESA3-Cub-PLV or CESA6-Cub-PLV, the expression of reporter genes was detected, suggesting that full-length μ2 and μ2MHD can interact with CESA3 and CESA6 (Fig. 1A, columns 7–10). As an additional negative control, no reporter gene expression was detected when either μ2-NubG or μ2MHD-NubG was cotransformed with Cub-PLV alone (Fig. 1A, columns 5 and 6).

To validate the interaction between μ2MHD and the primary CESAs further, in vitro pull-down assays were performed. Despite numerous attempts, we were unable to express full-length CESA proteins in *Escherichia coli*. Therefore, the central domains of primary CESAs were used in the pull-down assays. GST-μ2MHD was able to pull down His-CESA1CD, His-CESA3CD, and His-CESA6CD (Fig. 1B). No detectable His-CESACD proteins were pulled down by purified glutathione *S*-transferase (GST). These data suggest that μ2MHD mediates the interaction between μ2 and the central domain of CESA1, CESA3, and CESA6.

Characterization of μ2 Mutants and the Expression of μ2

To investigate the role of μ2 in Arabidopsis, two available transfer DNA (T-DNA) insertion lines for μ2 were obtained from the Arabidopsis Biological Resource Center. The SALK_083693 line (*μ2-1*) contained a T-DNA insertion at the splice site between the fourth exon and the fourth intron, and the SAIL_165_A05 line

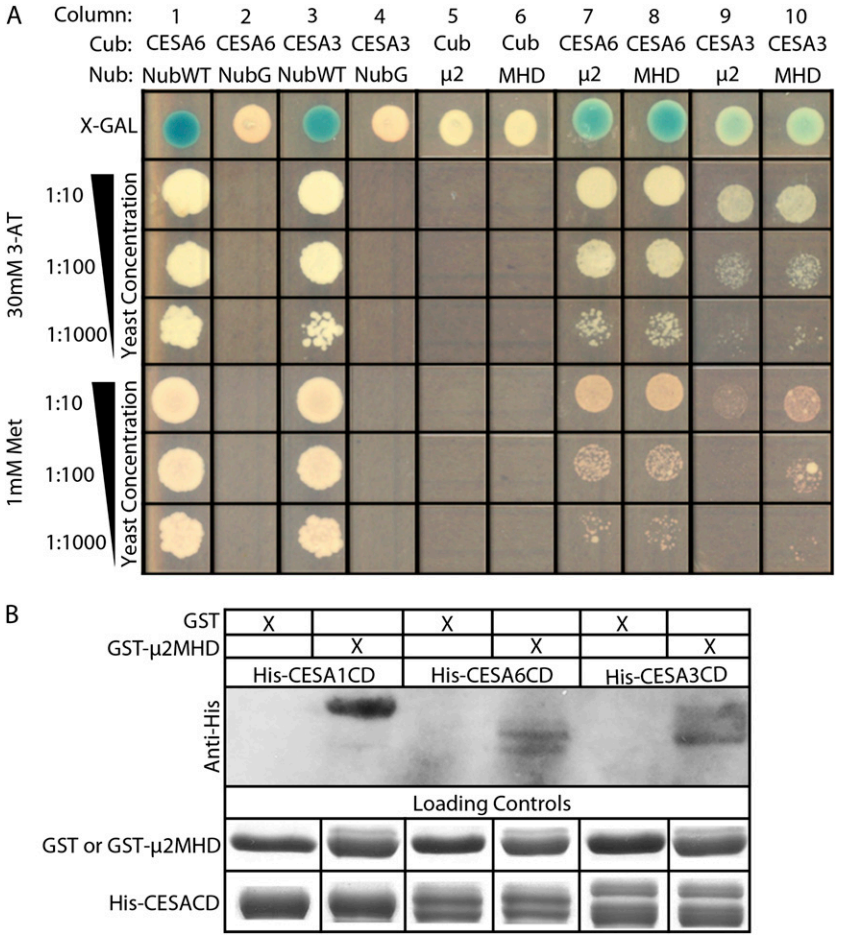

Figure 1. $\mu 2$ interacts with primary CESAs through the μ-homology domain. A, SU-Y2H analysis shows a positive interaction between $\mu 2$ and both CESA3 and CESA6. Interactions were selected on Leu-, Trp-, and His-dropout medium with 1.0 mM Met or 30 mM 3-ammonium-triazole (3-AT). 5-Bromo-4-chloro-3-indolyl-β-D-galactopyranoside (X-Gal) was added for the detection of β-galactosidase activity. Yeast strains were cotransformed with a Cub vector and a Nub vector. Cub vectors consisted of CESA6-Cub-PLV, CESA3-Cub-PLV, or Cub-PLV alone as a negative control. Nub vectors consisted of $\mu 2$-NubG or $\mu 2$MHD-NubG as experimental constructs and NubWT alone and NubG alone as positive and negative controls, respectively. B, $\mu 2$MHD interacts with the central domain of CESA1, CESA3, and CESA6 in vitro. His-CESA1CD, His-CESA3CD, and His-CESA6CD all coprecipitated with GST-$\mu 2$MHD. GST alone did not pull down His-CESA1CD, His-CESA3CD, or His-CESA6CD.

($\mu 2$-*2*) contained a T-DNA insertion in the seventh exon (Supplemental Fig. S2A). Homozygous $\mu 2$-*1* and $\mu 2$-*2* mutants lacked detectable transcripts as analyzed by reverse transcription-PCR (Supplemental Fig. S2B) and, therefore, were concluded to be null alleles. $\mu 2$-*1* and $\mu 2$-*2* shared similar phenotypes; therefore, only $\mu 2$-*1* was used for functional analysis of $\mu 2$.

Scanning electron microscopy of $\mu 2$-*1* pollen grains showed irregular or collapsed cell wall morphologies (Supplemental Fig. S2C), similar to the phenotypes reported for null mutants of *CESA1* and *CESA3* (Persson et al., 2007). Compared with wild-type seedlings, $\mu 2$-*1* seedlings had longer primary roots and etiolated hypocotyls (Supplemental Fig. S2, D–G). In 4- to 8-d-old light-grown seedlings, $\mu 2$-*1* roots were approximately 20% longer than those of wild-type seedlings. Likewise, in 4- to 7-d-old dark-grown seedlings, $\mu 2$-*1* hypocotyls were 15% to 20% longer than those of wild-type seedlings. In contrast, adult $\mu 2$-*1* plants were smaller in stature than wild-type plants and siliques of $\mu 2$-*1* plants were shorter and thinner than wild type-siliques (Supplemental Fig. S2, H–K).

The widespread mutant phenotypes of $\mu 2$-*1* suggest that $\mu 2$ plays a role in many tissues, which is consistent with the ubiquitous expression of $\mu 2$ obtained from Genevestigator. To obtain a detailed expression profile of $\mu 2$, the 1.5-kb region upstream of $\mu 2$ was fused to the *GUS* gene and transformed into wild-type plants. A histochemical analysis of GUS activity was performed in the transgenic plants. GUS expression from p$\mu 2$:*GUS* was detected in dark-grown hypocotyls, rosette leaves, stamen, pollen, developing siliques, and roots (Supplemental Fig. S3).

$\mu 2$ Is Involved in CME

The internalization of FM4-64, a membrane-impermeable fluorescent styryl dye, is commonly used to visualize general endocytosis in plant cells (Bolte et al., 2004; Dettmer et al., 2006; Dhonukshe et al., 2007; Lam et al., 2007; Collings et al., 2008; Viotti et al., 2010; Kitakura et al., 2011; Beck et al., 2012; Wang et al., 2013). It has been shown previously that small bright intracellular FM4-64 puncta with TGN/EE localization are visible after short exposure of root cells to FM4-64 (Dettmer et al., 2006) and that uptake of FM4-64 can be quantified under these conditions (Kitakura et al., 2011). Therefore, the general endocytic efficiency of $\mu 2$-*1* and wild-type seedlings was quantified in root epidermal cells after a short (8.5-min) exposure to 2 μM FM4-64. Wild-type seedlings showed many bright intracellular FM4-64 puncta, while $\mu 2$-*1* seedlings showed fewer intracellular FM4-64

puncta that were of lower intensity (Fig. 2A). Quantification of the internalization of FM4-64 revealed that *μ2-1* cells exhibited an approximately 45% decrease in FM4-64 internalization compared with the wild type (Fig. 2, B and C), supporting the role of μ2 in general endocytosis in Arabidopsis.

To examine the subcellular localization of μ2, a *μ2-YFP* (for yellow fluorescent protein) construct containing an approximately 1-kb native *μ2* promoter, genomic *μ2* sequence, and a C-terminal YFP tag was transformed into *μ2-1* plants. μ2-YFP fully complemented the FM4-64 internalization defect of the *μ2-1* mutant (Fig. 2) and the *μ2-1* mutant phenotype of dark-grown hypocotyls (Supplemental Fig. S4C), suggesting that the μ2-YFP fusion protein was functional. In dark-grown hypocotyls, μ2-YFP localized to the plasma membrane with punctate distribution and exhibited temporal behavior of appearance and disappearance (Supplemental Fig. S4, A and B; Supplemental Movie S1). The distribution and temporal behavior of μ2-YFP was similar to what has been observed for CLC and dynamin-related proteins (Konopka et al., 2008; Konopka and Bednarek, 2008; Fujimoto et al., 2010), suggesting that μ2-YFP might have a role in CME. To test the involvement of μ2 in CME, the μ2-YFP line was crossed with a CLC-mOrange line (Konopka et al., 2008). In dark-grown hypocotyls, both μ2-YFP and CLC-mOrange localized to the plasma membrane with punctate distribution and extensive colocalization (Fig. 3A). Colocalization ratios between μ2-YFP and CLC-mOrange were significantly higher than what is expected by coincident colocalization between randomly distributed particle populations of the same density (Supplemental Table S1). Both μ2-YFP and CLC-mOrange particles exhibited transient behavior such that particles appeared and disappeared at the plasma membrane while exhibiting minimal lateral movement. By documenting the temporal behavior of colocalized particles, it was observed that μ2-YFP and CLC-mOrange particles appeared and disappeared either within the same frame or within 5 s of one another (Fig. 3B; Supplemental Movie S2). The mean lifetimes of μ2-YFP and CLC-mOrange particles at the plasma membrane showed some variation (Fig. 3C), with average lifetimes of 24 ± 8 and 19 ± 7 s, respectively (Fig. 3D). The localization and temporal behavior of μ2-YFP and CLC-mOrange in dark-grown hypocotyls are similar to those of CLC and dynamin-related proteins (DRP1A and DRP2B) in other cell types that have been observed in previous studies (Konopka et al., 2008; Konopka and Bednarek, 2008; Fujimoto et al., 2010), which provides support for μ2 playing a role in CME.

μ2 and CESA Are Functionally Associated

A cross between mCherry-CESA6 and μ2-YFP lines was performed in order to observe the relationship between CESA6 and μ2 in planta. Like other fluorescent protein-CESA6 fusions (Paredez et al., 2006; Desprez et al., 2007), plasma membrane-localized mCherry-CESA6 formed small puncta that traveled bidirectionally at constant velocities in linear trajectories. μ2-YFP and mCherry-CESA6 particles both localized to distinct foci at the plasma membrane (Fig. 4). Although a small subset of plasma membrane-localized μ2-YFP and mCherry-CESA6 particles were colocalized, the colocalization ratio between the two particle populations was not significantly different from what is expected by coincident overlap of randomly distributed particles (Supplemental Table S1). This observation is consistent with the transient and infrequent nature that would be expected of CESA endocytosis. To investigate whether μ2-YFP and mCherry-CESA6 particles were functionally associated with one another, we observed the temporal behavior of colocalized particles. In some cases, the transient formation and disappearance of μ2-YFP particles was synchronized with a corresponding disappearance or depletion of mCherry-CESA6 fluorescence (Fig. 5; Supplemental Movie S3). These events suggest that μ2-YFP and mCherry-CESA6 are functionally associated at the plasma membrane, where CESAs can be endocytosed through a μ2-mediated mechanism.

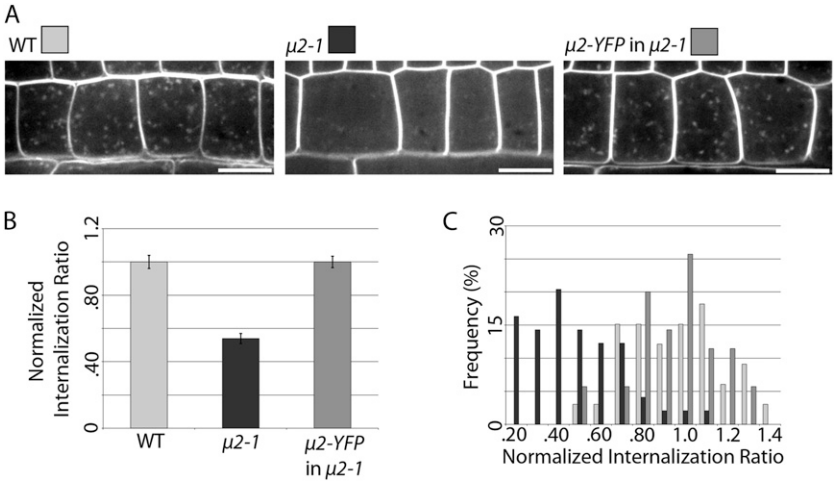

Figure 2. The *μ2-1* mutant has a defect in endocytosis that can be complemented by μ2-YFP. A, Intracellular FM4-64 puncta were imaged after 8.5 min of exposure to 2 μM FM4-64 in epidermal root cells in wild-type (WT), *μ2-1*, and μ2-YFP *μ2-1* seedlings. Bars = 10 μm. B, FM4-64 internalization was quantified (see "Materials and Methods") and normalized to the wild type (n = 33 cells, 16 seedlings for the wild type, 49 cells, 19 seedlings for *μ2-1*, and 35 cells, 12 seedlings for μ2-YFP *μ2-1*; $P < 0.0001$). Error bars represent SE. C, A histogram shows the distribution of FM4-64 internalization ratios.

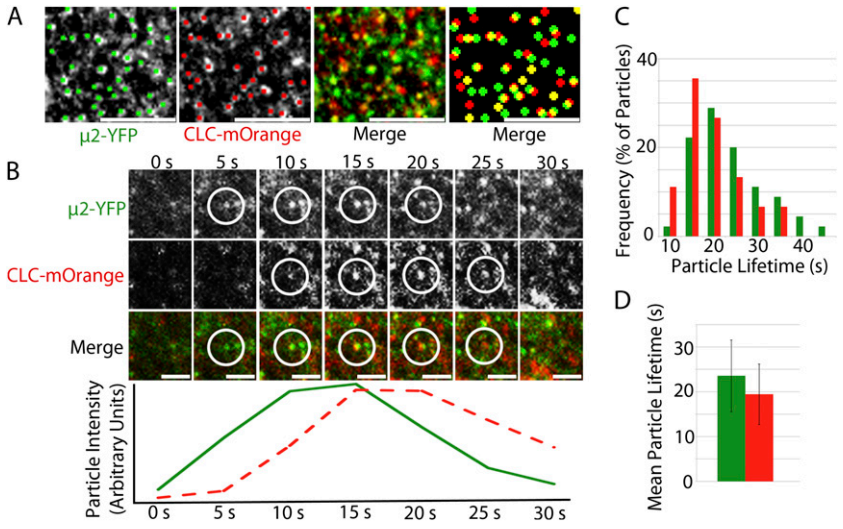

Figure 3. μ2-YFP and CLC-mOrange puncta colocalize and exhibit transient behavior at the plasma membrane with similar temporal behavior. A, Single-frame images show colocalization between μ2-YFP and CLC-mOrange particles at the plasma membrane. Manual particle selection was used to enhance the detection of colocalized particles. The left merge image displays two signals without manual particle selection, while the right merge image displays enlarged manually selected particles. Bars = 5 μm. B, Colocalized μ2-YFP and CLC-mOrange particles appear and disappear together at the plasma membrane. The fluorescence intensity profiles of the μ2-YFP (green trace) and CLC-mOrange (red dashed trace) are displayed in arbitrary units below the images for each time point. Shown is one representative instance chosen from more than 100 documented events. C, A histogram shows the distribution of μ2-YFP and CLC-mOrange particle lifetimes at the plasma membrane. D, Mean lifetime of μ2-YFP and CLC-mOrange particles (n = 45 particles for each μ2-YFP and CLC-mOrange). Error bars represent SD.

Interestingly, μ2-YFP also localized to intracellular compartments that exhibited cytoplasmic streaming behavior and overlapped with mCherry-CESA6-labeled compartments (Fig. 4). Mammalian μ2 is believed to be exclusively involved in endocytosis at the plasma membrane, while other μ homologs mediate trafficking at intracellular compartments. The localization of μ2-YFP to intracellular compartments in Arabidopsis may represent a plant-specific role of μ2.

YFP-CESA6 Density at the Plasma Membrane Is Dependent on μ2

If μ2 mediates the internalization of CESAs, the endocytosis defect of *μ2-1* would be expected to affect the distribution of CESAs at the plasma membrane. To investigate the distribution of CESAs, a line expressing YFP-CESA6, which complements the *prc1-1* mutation (Paredez et al., 2006), was crossed with *μ2-1*. The consequent YFP-CESA6 line with a homozygous *μ2-1*

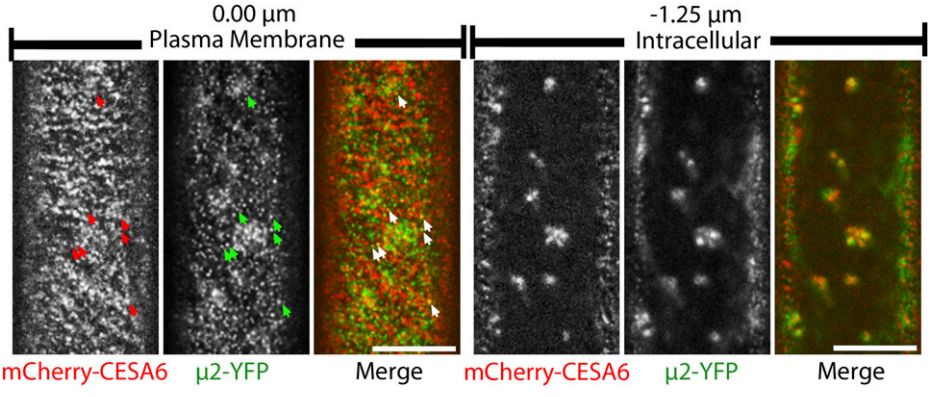

Figure 4. μ2-YFP and mCherry-CESA6 have overlapping distributions in planta. Confocal optical sections show epidermal cells of a 3-d-old etiolated hypocotyl coexpressing mCherry-CESA6 and μ2-YFP. mCherry-CESA6 and μ2-YFP puncta are visible at the plasma membrane (left) and in intracellular compartments (right). Arrows indicate examples of colocalized particles at the plasma membrane. Intracellular images were obtained at a focal plane that is 0.75 to 1.25 μm below the plasma membrane. Bars = 10 μm.

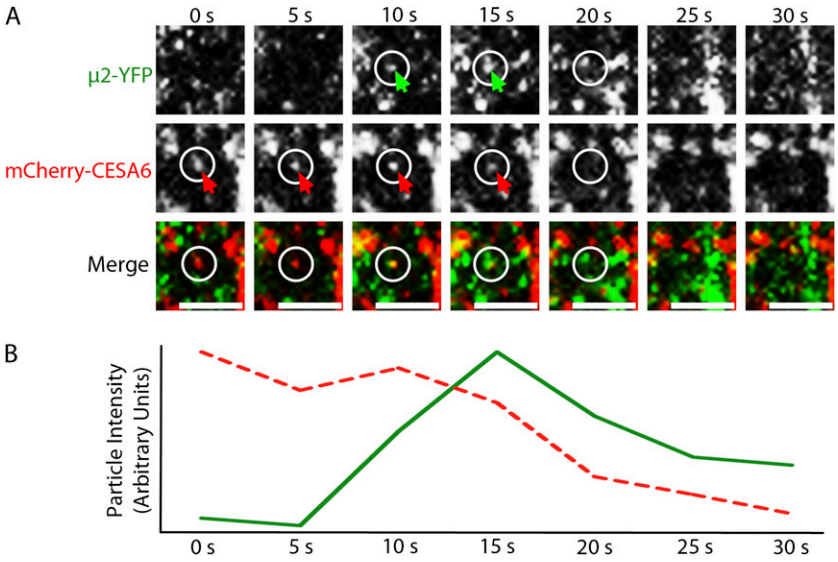

Figure 5. Plasma membrane-localized mCherry-CESA6 and μ2-YFP particles transiently colocalize before disappearing together. A, A time series of images shows the appearance of a μ2-YFP particle at the same position as an mCherry-CESA6 particle and the subsequent codisappearance of the particles at the 20-s frame. Arrows indicate μ2-YFP and mCherry-CESA6 particles. At the 20-s frame, circles mark the positions from which the particles disappeared. A μ2-YFP particle that forms above the position of the internalization event remains visible in subsequent frames, indicating that the focal plane is stable. Bars = 2 μm. B, Fluorescence intensity profiles of mCherry-CESA6 (red dashed trace) and μ2-YFP (green trace) particles are displayed in arbitrary units and show an association between the transient appearance and disappearance of the μ2-YFP particle and the diminishment of the mCherry-CESA6 particle intensity. Shown is one representative instance of a dozen documented events.

and *prc1-1* background was compared with a YFP-CESA6 control line that was homozygous for *prc1-1*. To prevent interference from intracellular YFP-CESA6 while analyzing the plasma membrane-localized YFP-CESA6 population, only regions of interest (ROIs) that were devoid of underlying intracellular YFP-CESA6 signal were analyzed (Fig. 6A). To aid in identifying ROIs that lacked intracellular YFP-CESA6 fluorescence, an image (red) was obtained from the focal plane just beneath the plasma membrane (approximately 0.75–1.25 μm under the plasma membrane plane) immediately after the acquisition of each plasma membrane-localized YFP-CESA6 image (green). The distribution of grayscale values from YFP-CESA6 *μ2-1 prc1-1* ROIs showed greater fluorescence intensity than ROIs in YFP-CESA6 *prc1-1* seedlings (Fig. 6B). In addition, the mean grayscale value of YFP-CESA6 in ROIs was significantly higher in the *μ2-1 prc1-1* background compared with the *prc1-1* control (Fig. 6C). The particle density of plasma membrane-localized YFP-CESA6 was measured by dividing the number of local foci maxima detected in each ROI by the area of the ROI. Particle density in the *μ2-1 prc1-1* background was 1.61 $\pm$ 0.15 particles μm^{-2} compared with 1.26 $\pm$ 0.12 particles μm^{-2} in the *prc1-1* background (Fig. 6D). These observations show that *μ2-1* mutant seedlings have more YFP-CESA6 at the plasma membrane, which may result from the endocytosis defect of *μ2-1*.

The Delivery Rate of YFP-CESA6 Particles Is Not Affected in *μ2-1*

The increased number of YFP-CESA6 particles at the plasma membrane in the *μ2-1 prc1-1* background could result from reduced endocytosis of CESAs, increased delivery of CESAs, or both. The delivery rate of YFP-CESA6 in *μ2-1 prc1-1* and *prc1-1* seedlings was measured by quantifying the delivery of YFP-CESA6 particles within a photobleached ROI during a 5-min period after photobleaching. As intracellular CESA compartments streamed through the ROI, plasma membrane-localized YFP-CESA6 particles reappeared within the bleached area. Similar to previous studies, these plasma membrane-localized particles often exhibited a period of stationary behavior before moving at constant velocities (Gutierrez et al., 2009; Bringmann et al., 2012). Only newly delivered particles and not laterally mobile particles from the perimeter of the bleached ROI were quantified. The delivery rate of YFP-CESA6 particles was similar in *μ2-1 prc1-1* and *prc1-1* backgrounds (1.86 $\pm$ 0.22 and 1.83 $\pm$ 0.21 particles μm^{-2} h^{-1}, respectively; Fig. 7; Supplemental Movie S4). These delivery rates were comparable to previous studies (Gutierrez et al., 2009; Bringmann et al., 2012). These data show that *μ2-1* does not affect the rate of YFP-CESA6 delivery to the plasma membrane. Therefore, the elevated density of YFP-CESA6 particles in the *μ2-1 prc1-1* background likely results from a reduction in the endocytosis of CESAs due to a lack of μ2 function.

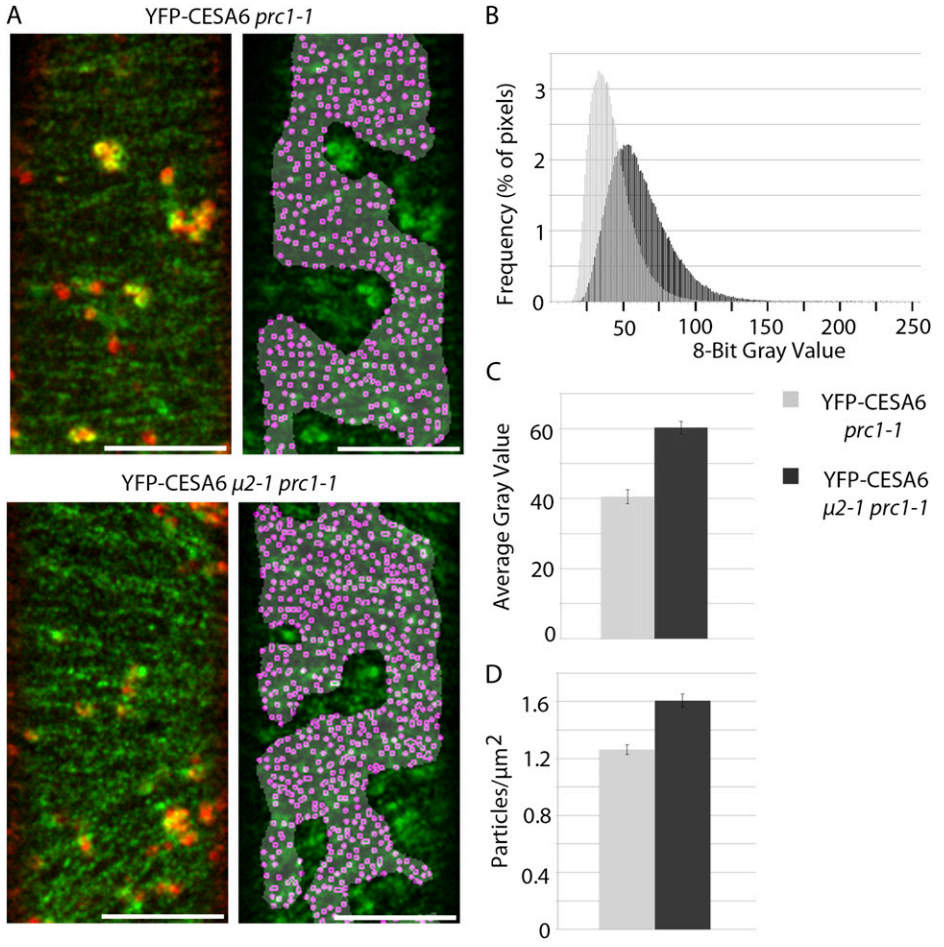

Figure 6. The *μ2-1* mutant has a higher density of CESAs at the plasma membrane. A, Representative images of the plasma membrane-localized YFP-CESA6 particles in *μ2-1 prc1-1* and the *prc1-1* control. Merged images between the plasma membrane (green) and intracellular (red) focal planes indicate the locations of intracellular compartments underlying the plasma membrane (left). A gray mask indicates the ROI lacking underlying intracellular compartments, and magenta dots indicate local maxima of the fluorescence signal (right). Bars = 10 μm. B to D, Quantification of YFP-CESA6 at the plasma membrane in *μ2-1 prc1-1* (dark gray bars) and *prc1-1* (light gray bars) genetic backgrounds. A histogram of the distribution of grayscale values of YFP-CESA6 signal (B), a graph of the mean grayscale value of YFP-CESA6 signal (C), and a graph of the average density of YFP-CESA6 particles (D) are shown (n = 11 cells from nine seedlings for *μ2-1 prc1-1* and 13 cells from 11 seedlings for *prc1-1*; $P < 0.0001$). Error bars represent SE.

The Velocity of YFP-CESA6 Particles Is Not Affected in *μ2-1*

To investigate whether the increased density of CESAs at the plasma membrane in *μ2-1* influenced the behavior of CESAs, the motility of plasma membrane-localized YFP-CESA6 particles was measured in both the *μ2-1 prc1-1* and *prc1-1* genetic backgrounds. In both lines, YFP-CESA6 particles traveled bidirectionally at constant velocities along linear tracks that can be visualized in averaged projections of 5-min time-lapse images (Supplemental Fig. S5A). In spite of the increased YFP-CESA6 particle density in the *μ2-1 prc1-1* background, the velocity distribution for CESA particles was similar in both *μ2-1 prc1-1* and *prc1-1* genetic backgrounds, with average velocities of 311 ± 188 nm min^{-1} in *μ2-1 prc1-1* and 322 ± 177 nm min^{-1} in *prc1-1* (Supplemental Fig. S5B; Supplemental Movie S5). This observation suggests that although the distribution of CESAs is affected by *μ2-1*, the function of YFP-CESA6 at the plasma membrane may not be significantly affected by *μ2-1*.

DISCUSSION

Although the existence and behavior of various CESA-containing cellular compartments have been observed using freeze-fracture transmission electron microscopy of rosette CSCs and live cell imaging of fluorescently tagged CESAs (Haigler and Brown, 1986; Paredez et al., 2006; Desprez et al., 2007; Crowell et al., 2009; Gutierrez et al., 2009), the mechanistic details of CESA trafficking to and from the plasma membrane have remained vague. Our results show that plant cells might regulate cellulose synthesis by controlling the abundance of active CSCs at the plasma membrane via μ2-mediated endocytosis.

μ2 Participates in CME and May Have Additional Roles at Intracellular Compartments

Several lines of evidence suggest that μ2-mediated endocytosis represents at least a subset of CME. First, μ2-YFP localized to the same transient foci as CLC-mOrange at the plasma membrane, and μ2-YFP puncta exhibited the same spatiotemporal behavior as CLC-mOrange puncta. Furthermore, the *μ2-1* mutant exhibited a significant FM4-64 internalization defect, which was consistent with the reduced uptake of FM4-64 in CME-defective seedlings (Kitakura et al., 2011). This FM4-64 internalization defect of *μ2-1* was complemented by μ2-YFP. In addition to having an endocytic defect, *μ2-1* seedlings also showed an enhanced dark-grown

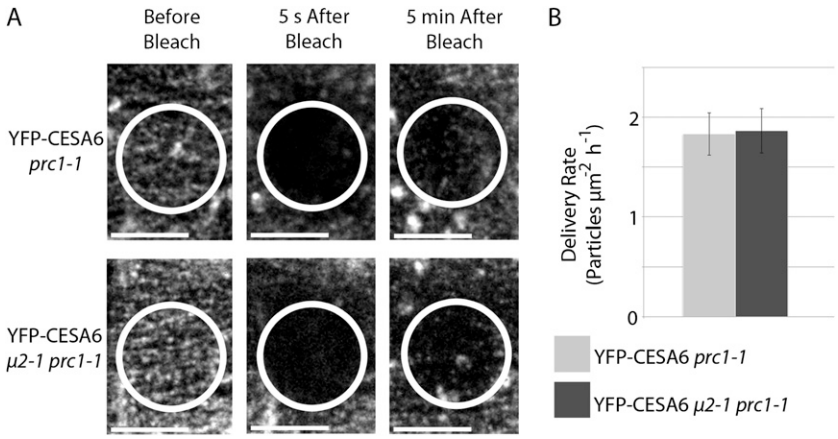

Figure 7. The delivery rate of YFP-CESA6 is similar in *μ2-1 prc1-1* and the *prc1-1* control. A, Representative images show the repopulation of the plasma membrane with YFP-CESA6 particles during the 5 min after the photobleaching of a ROI. Large signals from intracellular YFP-CESA6 that transiently passed through the ROI were not scored in the quantification of delivery. Bars = 10 μm. B, The quantification of the delivery rate shows no significant difference in the delivery of YFP-CESA6 in *μ2-1 prc1-1* (dark gray bar) and *prc1-1* (light gray bar) backgrounds (n = 5 seedlings for each *μ2-1 prc1-1* and *prc1-1*). Error bars represent SD.

hypocotyl-elongation phenotype and longer roots. Enhanced elongation of etiolated hypocotyls has also been documented for actin-binding protein mutants such as *actin depolymerizing factor4* and *capping protein* knockdown mutants (Henty et al., 2011; Li et al., 2012a). The involvement of actin in CME in yeast and mammals has been studied extensively (Boulant et al., 2011; Skruzny et al., 2012). Similarly, in plants, the use of actin and myosin drugs has been shown to affect the internalization of the flagellin receptor FLS2 (Robatzek et al., 2006; Beck et al., 2012), which suggests that a link between actin and endocytosis may also exist in plants. It has been shown that actin plays a role in the global distribution of CSCs (Gutierrez et al., 2009). Additional studies will be required to reveal whether alterations in the actin filament array or in the actin filament dynamics influence the μ2-mediated endocytosis of CSCs.

In mammals, μ2 is exclusively involved in trafficking from the plasma membrane and, therefore, is only localized to the plasma membrane and plasma membrane-derived vesicles. In contrast, Arabidopsis μ2 extensively localized to intracellular compartments in addition to the plasma membrane. These intracellular compartments exhibited cytoplasmic streaming and significant overlap with CESA-labeled compartments that are frequently referred to as Golgi bodies (Paredez et al., 2006; Crowell et al., 2009; Gutierrez et al., 2009; Gu et al., 2010; Gu and Somerville, 2010; Li et al., 2012b). This finding is consistent with a previous study in which μ2 (referred to as μA in that study) fractionated with AP complexes that localized to the Golgi/TGN (Happel et al., 2004). That study speculated that Golgi/TGN-localized μ2 might be involved in vacuolar trafficking (Happel et al., 2004); however, recent evidence suggests that vacuolar trafficking comes from the multivesicular body that is formed through maturation of the TGN/EE and not through trafficking from the Golgi/TGN (Scheuring et al., 2011). Although our study shows evidence for the involvement of μ2 in endocytosis at the plasma membrane, the function of μ2 at intracellular compartments remains unknown. In our study, the unaltered delivery rate of CESAs to the plasma membrane in the *μ2-1* mutant suggests that μ2 is not essential for the efficient secretion of CSCs to the plasma membrane. The Arabidopsis genome encodes four μ paralogs in addition to μ2 (Supplemental Table S2), two of which are 40% identical to μ2 in amino acid sequence (Boehm and Bonifacino, 2001). The relatively mild phenotype of *μ2-1* and the intracellular localization of μ2-YFP suggest that redundancy may exist between μ2 and other μ paralogs. The functional characterization of the remaining μ proteins will provide insight into the functional specificity and/or redundancy of μ proteins in Arabidopsis and may uncover significant differences between the AP complexes of mammals and plants.

CESA Distribution Is Dependent on μ2

Functional associations between μ2 and CSCs were displayed in multiple ways: (1) a direct interaction between μ2 or μ2MHD and the primary CESAs was shown in a SU-Y2H assay and in an in vitro pull-down assay; (2) μ2-YFP and mCherry-CESA6 colocalized at plasma membrane-localized particles and intracellular compartments; (3) plasma membrane-localized mCherry-CESA6 particles disappeared or diminished concomitantly with the transient appearance and disappearance of colocalized μ2-YFP particles; and (4) the endocytosis defect of *μ2-1* caused an increase in the amount of YFP-CESA6 at the plasma membrane without altering the rate of delivery of CSCs to the membrane. Together, these results suggest that some if not all CESAs are endocytosed through a CME mechanism. It remains to be tested whether the conservation between central domains of plant CESAs, in particular the class-specific region and/or the plant-conserved region, plays a role in cargo recognition.

There is evidence that the endocytosis frequency of CESAs is very low. Individual plasma membrane-localized YFP-CESA6 particles have been visualized to maintain constant velocities for an excess of 15 min (Paredez et al., 2006), but the direct observation of the lifetime of individual CESA particles at the plasma membrane is limited by the technical capabilities of live

cell imaging. By dividing our observed particle density measurement (about 1.25 particles μm^{-2}) by our observed YFP-CESA6 delivery rate measurement (about 1.8 particles $\mu m^{-2}\ h^{-1}$), we can estimate the lifetime of YFP-CESA6 particles to be approximately 40 min. By comparing the estimated lifetime of CESA particles with the observed average lifetime of μ2-YFP particles at the plasma membrane (about 25 s), we can estimate that only approximately 1% of CESA particles should be functionally associated with a μ2 particle and undergoing endocytosis at any given moment. This observation explains why the measured colocalization ratio between μ2-YFP and mCherry-CESA6 is not significantly different from the coincidental colocalization ratio between randomly distributed particles of the same density. The low colocalization ratio between μ2-YFP and mCherry-CESA6 can be further explained by the promiscuity of μ2, as it is expected to play a role in the endocytosis of a variety of cargoes in plants (Chen et al., 2011). In addition, CSCs might dissociate into smaller CESA aggregates of weak fluorescence intensity prior to being endocytosed, which might allude to the infrequency of imaging the endocytosis of CESA. In support of this idea, malformed or disintegrating rosette structures have been observed at the plasma membrane via transmission electron microscopy (Haigler and Brown, 1986). Despite the infrequency of CESA endocytosis, documentation of several incidents in which μ2-YFP and mCherry-CESA6 particles are functionally associated at the plasma membrane, and the observation that the abundance of YFP-CESA6 at the plasma membrane is increased in *μ2-1* provide strong evidence for the link between CESA and CME.

It remains to be investigated whether CESAs are degraded or recycled after being endocytosed. There is much evidence suggesting that CME cargo is transported to the TGN/EE (Dettmer et al., 2006; Viotti et al., 2010). If CESAs are trafficked to the TGN/EE upon endocytosis, it is possible that CESAs can be trafficked back to the plasma membrane. A recycling mechanism would be advantageous for the cell because the synthesis of a large protein complex such as the CSC would be costly. CSCs are delivered preferentially to cortical microtubules and subsequently move along cortical microtubule tracks (Paredez et al., 2006; Crowell et al., 2009; Gutierrez et al., 2009; Gu et al., 2010; Gu and Somerville, 2010; Li et al., 2012b). The endocytosis of malfunctioning or displaced CSCs and subsequent reassembly and recycling of these CSCs back to cortical microtubule positions at the plasma membrane might provide a mechanism by which plants can maintain the proper efficiency and organization of cellulose biosynthesis and deposition.

MATERIALS AND METHODS

Mutants and Transgenic Lines

The Arabidopsis (*Arabidopsis thaliana*) *μ2-1* homozygous line SALK_083693 was identified from the SIGnAL collection (Alonso et al., 2003) using primers listed in Supplemental Table S3. Seeds of SALK_083693 were obtained from the Arabidopsis Biological Resource Center at Ohio State University. Homozygous YFP-CESA6 *prc1-1* seeds (line A6Y-11) were obtained from Chris Somerville (Energy Bioscience Institute, University of California). YFP-CESA6 *prc1-1* was crossed with *μ2-1* to generate the YFP-CESA6 *μ2-1 prc1-1* line (YG103). *μ2-1* was genotyped via PCR (Supplemental Table S3), and *prc1-1* was genotyped by PCR followed by HpyCH4V digestion. To generate the *μ2-YFP* transgenic line, a genomic DNA fragment of *μ2* including a 1,027-bp promoter and the full-length coding region except for the 3′ untranslated region was amplified using primers listed in Supplemental Table S3 and cloned into the PCR8/GW/TOPO vector (Life Technologies). After sequencing, the genomic fragment of *μ2* was introduced into the pEarlyGate 311 vector (Arabidopsis Biological Resource Center) using Gateway LR Clonase (Invitrogen). The verified *μ2-YFP* (pYG108) construct was then introduced into *μ2-1* plants by *Agrobacterium tumefaciens*-mediated transformation. T2 homozygous lines (YG104 and YG105) were selected for further analysis. To generate the *mCherry-CESA6* transgenic line, the approximately 2-kb *CESA6* promoter was amplified with flanking *Hin*dIII and *Xba*I sites, cloned into the PCR8/GW/TOPO vector (Life Technologies), sequenced, and cloned into the pGWB2 vector using *Hin*dIII and *Xba*I (Supplemental Table S3). mCherry and the CESA6 coding sequence were amplified, ligated together at an introduced *Xba*I site, and cloned into the PCR8/GW/TOPO vector (Supplemental Table S3). After sequencing, mCherry-CESA6 was cloned into the pGWB2 vector that contained the native *CESA6* promoter using Gateway LR Clonase (Life Technologies) to produce pYG109. pYG109 was transformed into *prc1-1* by *A. tumefaciens*-mediated transformation and screened for hygromycin resistance, complementation of the *prc1-1* phenotype, and fluorescence. Transgenic lines selected for further analysis were designated YG106 and YG107.

SU-YTH Analysis

The full-length coding sequences of *CESA3*, *CESA6*, *μ2*, and *μ2MHD* were PCR amplified and cloned into the PCR8/GW/TOPO vector using primers in Supplemental Table S3. Sequenced *CESA* constructs were cloned into the bait *Cub-PLV* vector, *pMetYCgate* (Obrdlik et al., 2004), by Gateway cloning (Life Technologies). *pMetYCgate* harbors the *LEU2* gene for selection with Leu-dropout medium. Sequenced *μ2* constructs were cloned into the prey *Nub* vectors, *pXNgate21* and *pNXgate33*, by Gateway cloning (Life Technologies). *pXNgate21* and *pNXgate33* vectors contain the *TRP1* gene for selection with Trp-dropout medium. The prey expression was regulated by the *ADH1* promoter. The bait expression was regulated by the *Met-25* promoter, so the expression could be repressed by the addition of Met to increase the stringency of the assay.

The yeast strain *THY.AP4* was cotransformed with *Nub* and *Cub* constructs. Cotransformants were selected on synthetic medium lacking Leu and Trp. The interaction was selected on synthetic medium that lacked Leu, Trp, and His and contained 30 mM 3-ammonium-triazole or 1.0 mM Met to increase stringency. The β-galactosidase activity was determined by supplementing the medium with 80 mg L^{-1} 5-bromo-4-chloro-3-indolyl-β-D-galactopyranoside.

Protein Purification

The *μ2MHD* coding sequence was cloned into the *pGEX-KG* vector in frame with a GST tag and expressed in BL21Star-pLysS *Escherichia coli*. Protein expression was induced with 1 mM isopropyl β-D-1-thiogalactopyranoside at 30°C for 4 to 6 h. Protein purification was performed as described previously (Gu et al., 2006). The coding sequences of the central domains of *CESA1*, *CESA3*, and *CESA6* were cloned into YG201, which provides a His tag protein fusion, and expressed in BL21-CodonPlus (DE3)-RIPL *E. coli*. Protein was induced after a 30-min 15°C cold shock with 1 mM isopropyl β-D-1-thiogalactopyranoside at 15°C for 20 h. Protein purification was performed as described previously (Gu et al., 2006).

In Vitro Pull-Down Assay

Resin-bound GST-μ2MHD protein was washed twice in interaction buffer (20 mM HEPES, pH 7.4, 1 mM EDTA, 5 mM $MgCl_2$, 1 mM dithiothreitol, and 0.1% Triton X-100) for equilibration. Aliquots of approximately 2 μg of equilibrated resin-bound GST-μ2MHD protein were incubated with approximately 2 μg of soluble His-CESA1, His-CESA3, or His-CESA6 central domain protein in a total volume of 1 mL of interaction buffer for 2 h at 4°C on a rocker. The resin was then washed six times with interaction buffer, resuspended in SDS loading buffer, boiled, and subjected to SDS-PAGE and western blotting for analysis. On

western blots, His-CESA proteins were detected on film by chemiluminescence using a horseradish peroxidase-conjugated His antibody and SuperSignal West Femto substrate (Thermo).

FM4-64 Internalization Assay

FM4-64 (Invitrogen) was stored at −20°C in 10 mM stock aliquots in 100% dimethyl sulfoxide and diluted to 2 μM for use. FM4-64 was protected from light at all times. Seedlings were grown for 4 d on vertical Murashinge and Skoog plates (one-half-strength Murashinge and Skoog medium, 0.8% agar, 0.05% monohydrate MES, and 1% Suc, pH 5.7) on a 16-h-light/8-h-dark cycle at 22°C. Whole seedlings were incubated in 1 mL of 2 μM FM4-64 on a gentle rocker for 3 min prior to imaging. Slides were prepared with 2 μM FM4-64 solution, and images of root meristematic epidermal cells were obtained in 30-s increments at time points from 6.5 to 8.5 min after the initial introduction into FM4-64 (3.5–5.5 min after a 3-min FM4-64 incubation).

FM4-64 internalization was quantified using ImageJ software (W. Rasband, National Institutes of Health). Three values were obtained from each individually analyzed cell: the mean intensity of the plasma membrane signal, the mean intensity of the entire cytosol, and the mean intensity of an area of the cytosol lacking observable FM4-64 particles (background intensity). To calculate the uptake values, the mean background intensity was subtracted from the mean cytosolic intensity and the difference was divided by the mean plasma membrane intensity of each cell. Uptake values were normalized by dividing each uptake value by the average uptake value of the wild-type samples.

Live Cell Imaging

Etiolated hypocotyls were grown on vertical Murashinge and Skoog plates lacking Suc in the dark at 22°C for 3 d. Images were obtained of epidermal cells within 2 mm of the apical hook. Imaging was performed on a Yokogawa CSUX1 spinning-disk system featuring a DMI6000 Leica motorized microscope, a Photometrics QuantEM:512SC CCD camera, and a Leica 100×/1.4 numerical aperture oil objective. An ATOF laser with three laser lines (440/491/561 nm) was used to enable fast shuttering and switching between different excitations. Band-pass filters (485/30 nm for cyan fluorescent protein, 520/50 nm for GFP, 535/30 nm for YFP, and 620/60 nm for red fluorescent protein) were used for emission filtering. Image analysis was performed using Metamorph (Molecular Devices), ImageJ, and Imaris (Bitplane) software.

For plasma membrane CESA particle density measurements, a single optical section image was obtained at the plasma membrane followed by a second image at the Golgi plane about 1 μm below the membrane focal plane. The Golgi image was used as a reference in selecting a ROI of plasma membrane-localized CESA that lacked underlying Golgi fluorescence in order to avoid interference from Golgi-localized CESA. The area of the ROI was measured with ImageJ. The histogram tool in ImageJ was used to record the grayscale values of all pixels within the ROI of eight-bit images. The "find maxima" tool of ImageJ was used for particle detection within the ROI. An identical noise threshold was used for all analyses and was visually inspected for accurate representation of the particles.

For CESA particle dynamics analysis, a time series was obtained with a time interval of 5 s and a duration of 5 min. In ImageJ, the average intensity projection of the 5-min time-series images was used to visualize the tracks followed by CESA particles. Velocities of CESA particles along these tracks were measured in ImageJ using kymographs. Velocity measurements that were made computationally in Imaris were in agreement with the ImageJ measurements and used for analysis.

For the colocalization analyses, the overlap of manually selected plasma membrane-localized particles within a ROI was analyzed as a percentage of one particle population that overlapped with the other and vice versa. Pearson correlation coefficients were calculated in ImageJ using the Pearson–Spearman correlation colocalization plugin as described (French et al., 2008). The colocalization coincidence expected by the random distribution of particles was calculated by performing the same analyses on images in which one channel was rotated 180° relative to the other. The F1 line of the μ2-YFP/CLC-mOrange cross and the F2 line of the μ2-YFP/mCherry-CESA6 cross were analyzed.

Sequence data from this article can be found in the GenBank/EMBL data libraries under accession numbers listed in Supplemental Table S2.

Supplemental Data

The following materials are available in the online version of this article.

Supplemental Figure S1. μ2 was identified as a putative CESA6-interactive protein using a conventional YTH screen.

Supplemental Figure S2. The *μ2-1* mutant shows morphological phenotypes.

Supplemental Figure S3. *μ2* is ubiquitously expressed.

Supplemental Figure S4. μ2-YFP complements *μ2-1*, has punctate distribution at the plasma membrane, and exhibits appearing and disappearing behavior at the plasma membrane.

Supplemental Figure S5. YFP-CESA6 motility is similar in the *μ2-1 prc1-1* and *prc1-1* backgrounds.

Supplemental Table S1. Colocalization quantification of μ2-YFP/CLC-mOrange and μ2-YFP/mCherry-CESA6.

Supplemental Table S2. Homology between Arabidopsis μ proteins and human μ2 protein and between Arabidopsis μ proteins and Arabidopsis μ2.

Supplemental Table S3. Primers used in this study.

Supplemental Movie S1. μ2-YFP particles display transient appearing and disappearing behavior at the plasma membrane.

Supplemental Movie S2. Colocalized μ2-YFP and CLC-mOrange particles exhibit the same temporal behavior.

Supplemental Movie S3. The disappearance of a plasma membrane-localized mCherry-CESA6 particle occurs with the concomitant appearance and disappearance of a colocalized μ2-YFP particle.

Supplemental Movie S4. The delivery of YFP-CESA6 particles within a photobleached region is shown during a 5-min interval after bleaching.

Supplemental Movie S5. The dynamics of plasma membrane-localized YFP-CESA6 particles is similar in *prc1-1* and *μ2-1 prc1-1* genetic backgrounds.

ACKNOWLEDGMENTS

We gratefully acknowledge support during the initiation of this research from Chris Somerville and the Energy Biosciences Institute. We thank S. Bednarek for providing CLC-mOrange transgenic lines and C. Somerville for providing YFP-CESA6 transgenic lines.

Received May 9, 2013; accepted July 8, 2013; published July 12, 2013.

LITERATURE CITED

Alonso JM, Stepanova AN, Leisse TJ, Kim CJ, Chen HM, Shinn P, Stevenson DK, Zimmerman J, Barajas P, Cheuk R, et al (2003) Genome-wide insertional mutagenesis of Arabidopsis thaliana. Science **301:** 653–657

Baluska F, Hlavacka A, Samaj J, Palme K, Robinson DG, Matoh T, McCurdy DW, Menzel D, Volkmann D (2002) F-actin-dependent endocytosis of cell wall pectins in meristematic root cells: insights from brefeldin A-induced compartments. Plant Physiol **130:** 422–431

Baluska F, Liners F, Hlavacka A, Schlicht M, Van Cutsem P, McCurdy DW, Menzel D (2005) Cell wall pectins and xyloglucans are internalized into dividing root cells and accumulate within cell plates during cytokinesis. Protoplasma **225:** 141–155

Bandmann V, Homann U (2012) Clathrin-independent endocytosis contributes to uptake of glucose into BY-2 protoplasts. Plant J **70:** 578–584

Beck M, Zhou J, Faulkner C, MacLean D, Robatzek S (2012) Spatio-temporal cellular dynamics of the *Arabidopsis* flagellin receptor reveal activation status-dependent endosomal sorting. Plant Cell **24:** 4205–4219

Boehm M, Bonifacino JS (2001) Adaptins: the final recount. Mol Biol Cell **12:** 2907–2920

Bolte S, Talbot C, Boutte Y, Catrice O, Read ND, Satiat-Jeunemaitre B (2004) FM-dyes as experimental probes for dissecting vesicle trafficking in living plant cells. J Microsc **214:** 159–173

Boulant S, Kural C, Zeeh JC, Ubelmann F, Kirchhausen T (2011) Actin dynamics counteract membrane tension during clathrin-mediated endocytosis. Nat Cell Biol **13:** 1124–1131

Bringmann M, Li E, Sampathkumar A, Kocabek T, Hauser MT, Persson S (2012) POM-POM2/cellulose synthase interacting1 is essential for the functional association of cellulose synthase and microtubules in *Arabidopsis*. Plant Cell **24:** 163–177

Brown DM, Zeef LA, Ellis J, Goodacre R, Turner SR (2005) Identification of novel genes in *Arabidopsis* involved in secondary cell wall formation using expression profiling and reverse genetics. Plant Cell **17:** 2281–2295

Chen X, Irani NG, Friml J (2011) Clathrin-mediated endocytosis: the gateway into plant cells. Curr Opin Plant Biol **14:** 674–682

Cocucci E, Aguet F, Boulant S, Kirchhausen T (2012) The first five seconds in the life of a clathrin-coated pit. Cell **150:** 495–507

Collings DA, Gebbie LK, Howles PA, Hurley UA, Birch RJ, Cork AH, Hocart CH, Arioli T, Williamson RE (2008) Arabidopsis dynamin-like protein DRP1A: a null mutant with widespread defects in endocytosis, cellulose synthesis, cytokinesis, and cell expansion. J Exp Bot **59:** 361–376

Crowell EF, Bischoff V, Desprez T, Rolland A, Stierhof YD, Schumacher K, Gonneau M, Höfte H, Vernhettes S (2009) Pausing of Golgi bodies on microtubules regulates secretion of cellulose synthase complexes in *Arabidopsis*. Plant Cell **21:** 1141–1154

Crowell EF, Gonneau M, Stierhof YD, Höfte H, Vernhettes S (2010) Regulated trafficking of cellulose synthases. Curr Opin Plant Biol **13:** 700–705

Desprez T, Juraniec M, Crowell EF, Jouy H, Pochylova Z, Parcy F, Höfte H, Gonneau M, Vernhettes S (2007) Organization of cellulose synthase complexes involved in primary cell wall synthesis in Arabidopsis thaliana. Proc Natl Acad Sci USA **104:** 15572–15577

Dettmer J, Hong-Hermesdorf A, Stierhof YD, Schumacher K (2006) Vacuolar H^+-ATPase activity is required for endocytic and secretory trafficking in *Arabidopsis*. Plant Cell **18:** 715–730

Dhonukshe P, Aniento F, Hwang I, Robinson DG, Mravec J, Stierhof YD, Friml J (2007) Clathrin-mediated constitutive endocytosis of PIN auxin efflux carriers in Arabidopsis. Curr Biol **17:** 520–527

French AP, Mills S, Swarup R, Bennett MJ, Pridmore TP (2008) Colocalization of fluorescent markers in confocal microscope images of plant cells. Nat Protoc **3:** 619–628

Fujimoto M, Arimura S, Ueda T, Takanashi H, Hayashi Y, Nakano A, Tsutsumi N (2010) Arabidopsis dynamin-related proteins DRP2B and DRP1A participate together in clathrin-coated vesicle formation during endocytosis. Proc Natl Acad Sci USA **107:** 6094–6099

Green PB (1962) Mechanism for plant cellular morphogenesis. Science **138:** 1404–1405

Gu Y, Kaplinsky N, Bringmann M, Cobb A, Carroll A, Sampathkumar A, Baskin TI, Persson S, Somerville CR (2010) Identification of a cellulose synthase-associated protein required for cellulose biosynthesis. Proc Natl Acad Sci USA **107:** 12866–12871

Gu Y, Li SD, Lord EM, Yang ZB (2006) Members of a novel class of *Arabidopsis* Rho guanine nucleotide exchange factors control Rho GTPase-dependent polar growth. Plant Cell **18:** 366–381

Gu Y, Somerville C (2010) Cellulose synthase interacting protein: a new factor in cellulose synthesis. Plant Signal Behav **5:** 1571–1574

Gutierrez R, Lindeboom JJ, Paredez AR, Emons AM, Ehrhardt DW (2009) Arabidopsis cortical microtubules position cellulose synthase delivery to the plasma membrane and interact with cellulose synthase trafficking compartments. Nat Cell Biol **11:** 797–806

Haigler CH, Brown RM Jr (1986) Transport of rosettes from the Golgi apparatus to the plasma membrane in isolated mesophyll cells of Zinnia elegans during differentiation to tracheary elements in suspension culture. Protoplasma **134:** 111–120

Happel N, Höning S, Neuhaus JM, Paris N, Robinson DG, Holstein SE (2004) Arabidopsis mu A-adaptin interacts with the tyrosine motif of the vacuolar sorting receptor VSR-PS1. Plant J **37:** 678–693

Henty JL, Bledsoe SW, Khurana P, Meagher RB, Day B, Blanchoin L, Staiger CJ (2011) *Arabidopsis* actin depolymerizing factor4 modulates the stochastic dynamic behavior of actin filaments in the cortical array of epidermal cells. Plant Cell **23:** 3711–3726

Holstein SE (2002) Clathrin and plant endocytosis. Traffic **3:** 614–620

Jackson LP, Kelly BT, McCoy AJ, Gaffry T, James LC, Collins BM, Höning S, Evans PR, Owen DJ (2010) A large-scale conformational change couples membrane recruitment to cargo binding in the AP2 clathrin adaptor complex. Cell **141:** 1220–1229

Kimura S, Laosinchai W, Itoh T, Cui X, Linder CR, Brown RM Jr (1999) Immunogold labeling of rosette terminal cellulose-synthesizing complexes in the vascular plant *Vigna angularis*. Plant Cell **11:** 2075–2086

Kitakura S, Vanneste S, Robert S, Löfke C, Teichmann T, Tanaka H, Friml J (2011) Clathrin mediates endocytosis and polar distribution of PIN auxin transporters in *Arabidopsis*. Plant Cell **23:** 1920–1931

Kleine-Vehn J, Friml J (2008) Polar targeting and endocytic recycling in auxin-dependent plant development. Annu Rev Cell Dev Biol **24:** 447–473

Konopka CA, Backues SK, Bednarek SY (2008) Dynamics of *Arabidopsis* dynamin-related protein 1C and a clathrin light chain at the plasma membrane. Plant Cell **20:** 1363–1380

Konopka CA, Bednarek SY (2008) Comparison of the dynamics and functional redundancy of the Arabidopsis dynamin-related isoforms DRP1A and DRP1C during plant development. Plant Physiol **147:** 1590–1602

Lam SK, Tse YC, Robinson DG, Jiang L (2007) Tracking down the elusive early endosome. Trends Plant Sci **12:** 497–505

Lei L, Li S, Gu Y (2012) Cellulose synthase interactive protein 1 (CSI1) mediates the intimate relationship between cellulose microfibrils and cortical microtubules. Plant Signal Behav **7:** 714–718

Li J, Henty-Ridilla JL, Huang S, Wang X, Blanchoin L, Staiger CJ (2012a) Capping protein modulates the dynamic behavior of actin filaments in response to phosphatidic acid in *Arabidopsis*. Plant Cell **24:** 3742–3754

Li S, Lei L, Somerville CR, Gu Y (2012b) Cellulose synthase interactive protein 1 (CSI1) links microtubules and cellulose synthase complexes. Proc Natl Acad Sci USA **109:** 185–190

McMahon HT, Boucrot E (2011) Molecular mechanism and physiological functions of clathrin-mediated endocytosis. Nat Rev Mol Cell Biol **12:** 517–533

Obrdlik P, El-Bakkoury M, Hamacher T, Cappellaro C, Vilarino C, Fleischer C, Ellerbrok H, Kamuzinzi R, Ledent V, Blaudez D, et al (2004) K^+ channel interactions detected by a genetic system optimized for systematic studies of membrane protein interactions. Proc Natl Acad Sci USA **101:** 12242–12247

Paredez AR, Somerville CR, Ehrhardt DW (2006) Visualization of cellulose synthase demonstrates functional association with microtubules. Science **312:** 1491–1495

Persson S, Paredez A, Carroll A, Palsdottir H, Doblin M, Poindexter P, Khitrov N, Auer M, Somerville CR (2007) Genetic evidence for three unique components in primary cell-wall cellulose synthase complexes in Arabidopsis. Proc Natl Acad Sci USA **104:** 15566–15571

Persson S, Wei H, Milne J, Page GP, Somerville CR (2005) Identification of genes required for cellulose synthesis by regression analysis of public microarray data sets. Proc Natl Acad Sci USA **102:** 8633–8638

Robatzek S, Chinchilla D, Boller T (2006) Ligand-induced endocytosis of the pattern recognition receptor FLS2 in Arabidopsis. Genes Dev **20:** 537–542

Samaj J, Baluska F, Voigt B, Schlicht M, Volkmann D, Menzel D (2004) Endocytosis, actin cytoskeleton, and signaling. Plant Physiol **135:** 1150–1161

Samaj J, Read ND, Volkmann D, Menzel D, Baluska F (2005) The endocytic network in plants. Trends Cell Biol **15:** 425–433

Scheuring D, Viotti C, Krüger F, Künzl F, Sturm S, Bubeck J, Hillmer S, Frigerio L, Robinson DG, Pimpl P, et al (2011) Multivesicular bodies mature from the trans-Golgi network/early endosome in *Arabidopsis*. Plant Cell **23:** 3463–3481

Skruzny M, Brach T, Ciuffa R, Rybina S, Wachsmuth M, Kaksonen M (2012) Molecular basis for coupling the plasma membrane to the actin cytoskeleton during clathrin-mediated endocytosis. Proc Natl Acad Sci USA **109:** E2533–E2542

Taylor NG, Howells RM, Huttly AK, Vickers K, Turner SR (2003) Interactions among three distinct CesA proteins essential for cellulose synthesis. Proc Natl Acad Sci USA **100:** 1450–1455

Taylor NG, Scheible WR, Cutler S, Somerville CR, Turner SR (1999) The *irregular xylem3* locus of *Arabidopsis* encodes a cellulose synthase required for secondary cell wall synthesis. Plant Cell **11:** 769–780

Viotti C, Bubeck J, Stierhof YD, Krebs M, Langhans M, van den Berg W, van Dongen W, Richter S, Geldner N, Takano J, et al (2010) Endocytic and secretory traffic in *Arabidopsis* merge in the trans-Golgi network/early endosome, an independent and highly dynamic organelle. Plant Cell **22:** 1344–1357

Wang C, Yan X, Chen Q, Jiang N, Fu W, Ma B, Liu J, Li C, Bednarek SY, Pan J (2013) Clathrin light chains regulate clathrin-mediated trafficking, auxin signaling, and development in *Arabidopsis*. Plant Cell **25:** 499–516

Wang J, Elliott JE, Williamson RE (2008) Features of the primary wall CESA complex in wild type and cellulose-deficient mutants of Arabidopsis thaliana. J Exp Bot **59:** 2627–2637

Xiong G, Li R, Qian Q, Song X, Liu X, Yu Y, Zeng D, Wan J, Li J, Zhou Y (2010) The rice dynamin-related protein DRP2B mediates membrane trafficking, and thereby plays a critical role in secondary cell wall cellulose biosynthesis. Plant J **64:** 56–70